Mapping cell migrations and fates in a gastruloid model to the human primitive streak

Iain Martyn[1,2], Eric D. Siggia[2,*] and Ali H. Brivanlou[1,*]

ABSTRACT

Although fate maps of early embryos exist for nearly all model organisms, a fate map of the gastrulating human embryo remains elusive. Here, we use human gastruloids to piece together a rudimentary fate map for the human primitive streak (PS). This is possible because differing levels of BMP, WNT and NODAL lead to self-organization of gastruloids into homogenous subpopulations of endoderm and mesoderm, and comparative analysis of these gastruloids, together with the fate map of the mouse embryo, allows the organization of these subpopulations along an anterior-posterior axis. We also developed a novel cell tracking technique that detected robust fate-dependent cell migrations in our gastruloids comparable with those found in the mouse embryo. Taken together, our fate map and recording of cell migrations provides a first coarse view of what the human PS may resemble *in vivo*.

KEY WORDS: Fate map, Gastruloid, Human, Migration, Primitive streak, Stem cell

INTRODUCTION

During amniote gastrulation a symmetrical sheet of identical cells rapidly transforms itself into a multi-layered structure with distinct cell fates and an anterior-posterior axis (Solnica-Krezel and Sepich, 2012). This process commences with the initiation of the primitive streak (PS), a transient structure that begins posteriorly and grows towards the center. As the streak grows, cells migrate through and give rise to different endodermal and mesodermal lineages. Specification of these different cell types depends on the position and time at which a cell transits through the streak.

A first step toward understanding gastrulation is to track the developmental path of each progenitor cell and learn what structures and lineages they contribute to at later times. This information can be represented graphically in a so-called 'fate map', on which cell location and fate can be marked. Although fate maps have been completed for most model organisms (Tam and Behringer, 1997; Hatada and Stern, 1994; Conklin, 1905; Vogt, 1929; Kimmel et al., 1990; Alev et al., 2010), no fate map exists for human. This is because of ethical reasons prohibiting culturing human embryos beyond 14-days *ex vivo*, the time when the PS first appears (Hyun et al., 2016; International Society of Stem Cell Research, 2016; Deglincerti et al., 2016). A map of the gastrulating human embryo, however, could be incredibly useful not only for comparison with

model organisms and for understanding development in general, but for the practical use to guide directed differentiation strategies of human embryonic stem cells (hESCs) into endoderm or mesoderm cell subtypes.

Given the restrictions, alternative strategies have been pursued. Recently, we have proposed a 'gastruloid' approach using hESCs that is robust and amenable to single cell quantification (Warmflash et al., 2014; Simunovic and Brivanlou, 2017; van den Brink et al., 2014). We have shown that when grown in epiblast-like geometrically confined disks, hESCs respond to BMP4 by differentiating and self-organizing into concentric rings of embryonic germ layers: with ectoderm in the center, extra-embryonic tissue at the edge, and mesoderm and endoderm in between. We have also shown that an evolutionarily conserved BMP→WNT→NODAL signaling hierarchy is responsible for this patterning, that WNT3A+activin stimulation results in an organizer-like cell population that can induce a secondary axis when grafted into a chick embryo (Martyn et al., 2018), and that negative feedback from DKK1 and boundary forces transduced by E-CAD (CDH1) control the WNT pattern (Martyn et al., 2019).

In this work, we use our gastruloids to construct a rudimentary fate map of the human PS. We find that different subpopulations of endoderm or mesoderm emerge depending on BMP, WNT and NODAL levels, and that by comparison with the mouse embryo we can arrange these subpopulations along an anterior-posterior axis. In the absence of direct characterization in the human gastrula, we rely heavily on mouse data to define markers for human cell types. We believe this assumption is safe as, regardless of the geometry, we have tried to use mutually exclusive sets of markers that always delineate the same cell type across multiple vertebrate species, and that have been used in recent successful mappings of mouse gastruloid cell populations to the mouse embryo (Morgani et al., 2018). We also find robust cell migrations from the PS region of each gastruloid that are dependent on cell fates, with fast single cell migrations in the case of endoderm and slower group migrations in the case of mesoderm. In some conditions, this migration correlates with the appearance of a collagen IV basement membrane separating the migrating cells and the epiblast layer they involute under, similar to the mouse embryo. Taken together, we believe our gastruloids offer a rich system through which a rudimentary fate map of the PS and picture of early human gastrulation can be pieced together.

RESULTS AND DISCUSSION
Anterior-posterior fate specification in human gastruloids

Building on our previous characterization of gastruloid cell fates (Warmflash et al., 2014) and incentivized by the discovery of a human organizer in WNT3A+activin-treated cells (Martyn et al., 2018), we hypothesized that other PS subtypes were present in our gastruloids and that they could also be compared with the anterior-posterior axis of the mouse embryo. Our hypothesis was supported by recent work mapping cell types in mouse gastruloids to mouse embryos (Morgani et al., 2018), in which particular combinations of

[1]Laboratory of Stem Cell Biology and Molecular Embryology, The Rockefeller University, New York, NY 10065, USA. [2]Center for Studies in Physics and Biology, The Rockefeller University, New York, NY 10065, USA.

*Authors for correspondence (siggiae@rockefeller.edu; brvnlou@rockefeller.edu)

I.M., 0000-0003-0868-3531; E.D.S., 0000-0001-7482-1854; A.H.B., 0000-0002-1761-280X

cell type-specific transcription factors were used to identify discrete fates and compare their pattern with the mouse embryo. Here, we follow the same strategy and analyze our BMP4-, WNT3A-, WNT3A+SB-431542 (SB)- or WNT3A+activin-induced human gastruloids at 24 h and 48 h for anterior-posterior identity and compare them with the mouse gene map and fate map at E7.5 (Fig. 1A,B and Fig. S1B).

Strikingly, we found largely homogenous anterior-posterior subpopulations that arose distinctly in one set of stimulation conditions and not the others. For example, only BMP4 induced expression of HAND1, CDX2 and GATA3, and these markers were all present in the same set of cells on the periphery of the gastruloid (Fig. 1C). In the mouse, HAND1 is first expressed at embryonic day (E)7.5 in the trophectoderm and extra-embryonic mesoderm, including the amnion, chorion, allantois and visceral yolk sac (Firulli et al., 1998). GATA3 is expressed in the mouse and human pre-implantation trophoblast (Deglincerti et al., 2016; Home et al., 2017; Ralston et al., 2010) and in the mouse E7.5 extra-embryonic ectoderm and allantois (Ralston et al., 2010; Manaia et al., 2000). CDX2 is also expressed in the mouse and human pre-implantation trophoblast (Deglincerti et al., 2016) and in mouse is restricted to the extra-embryonic ectoderm, mesoderm and posterior endoderm until E8.5 (Morgani et al., 2018; Beck et al., 1995; Sherwood et al., 2011). Based on these comparisons, we take this region of the BMP4-induced gastruloid to most closely resemble mouse E7.5 extra-embryonic mesoderm. This is further supported by the fact that there is a BMP source from the extra-embryonic ectoderm immediately adjacent to it *in vivo*. The fact that we do not see significant brachyury (BRA; T in mouse, TBXT in human) expression in these cells as observed in mouse (Morgani et al., 2018) may be owing to species-specific timing differences (for example, we have shown previously that there is a wave of BRA expression earlier in this region at 12-36h Warmflash et al., 2014). Radially central to this extra-embryonic mesoderm population are three other readily identifiable subpopulations that are unique to the BMP4 gastruloid. First, in the region adjacent to the extra-embryonic mesoderm there is a population of BRA+/GATA6+ cells (Fig. 1C). In the mouse at E7.5, GATA6 marks the parietal and definitive endoderm plus the lateral mesoderm (Morgani et al., 2018; Koutsourakis et al., 1999). Thus we identify this subpopulation as lateral mesoderm. Second, staining for SOX17 [a marker of definitive endoderm that appears at E7-7.5 (Morgani et al., 2018) in mouse epiblast cells that transit through the PS], NANOG [which plays a role in endodermal differentiation (Teo et al., 2011) and also marks the mouse posterior epiblast after implantation (Morgani et al., 2018; Hart et al., 2004)] and OTX2 [marker of anterior epiblast and anterior PS in mouse from E7 (Morgani et al., 2018)] detected a population of the SOX17+/NANOG–/OTX2– cells (Fig. 1C). Based on the expression of these markers, we identify this population as posterior endoderm. Finally, examining SOX2 (marker of ectoderm and pluripotency) and OCT4 (POU5F1; marker of epiblast) revealed a SOX2+/NANOG–/OCT4– subpopulation indicative of epiblast cells differentiating towards ectoderm (Fig. 1D). We term this subpopulation 'presumptive ectoderm'. Together, these four subpopulations in the BMP4 gastruloid all approximately match the E7.5 proximal posterior PS in mouse.

With WNT3A+SB stimulation we found expression of TBX6 in the region that co-expresses CDX2 and BRA (Fig. 1C). TBX6 did not appear in the other stimulation conditions, and using qPCR we also found that MSGN1 was induced with WNT3A+SB only (Fig. S1A). In the mouse, both TBX6 and MSGN1 are first expressed in the PS in the same region as BRA at E7.5, only to become restricted to paraxial mesoderm by E8.5 (Chapman et al.,

1996; Yoon et al., 2000; Chalamalasetty et al., 2014). The fact that we do not detect significant TBX6 or MSGN1 levels at earlier times in any of the other gastruloids in which we also see BRA (data not shown) may reflect a species-specific difference between human and mouse. In addition, although we use CDX2 in our panel of markers for the BMP4-induced gastruloids, CDX2 has also been shown to be crucial for paraxial mesoderm development in the mouse and is detectable there from E8.5 onwards (Beck et al., 1995; Savory et al., 2009). The union of TBX6, MSGN1 and CDX2 is thus highly suggestive of paraxial mesoderm, and a corresponding time of ~E7.5-8.5 in the mouse.

In the case of WNT3A and WNT3A+activin, stimulation led to co-expression of the transcription factors FOXA2 and OTX2 in the SOX17+ region at the edge (Fig. 1C). In the mouse, FOXA2 begins to be expressed in the anterior PS at E7, and becomes restricted to the anterior definitive endoderm and axial mesoderm by E7.75 (Morgani et al., 2018; Nowotschin et al., 2018preprint). Thus FOXA2+/ OTX2+/SOX17+/BRA– provides the signature of anterior endoderm. In addition, at 24 h with WNT3A+activin, but not WNT3A alone, we can detect the organizer marker GSC (Fig. 1C). As previously shown (Martyn et al., 2018), we can identify an organizer population at 24 h in WNT3A+activin gastruloids when GSC is co-expressed with BRA, and SOX17 is not yet visible (Fig. S2B). Finally, the centers of the WNT3A-, WNT3A+activin- and WNT3A+SB-stimulated gastruloids differ from the center region of the BMP4-stimulated gastruloids in that they still express NANOG and OCT4, albeit at a lower level than in pluripotency (Fig. 1C). We thus categorize these regions as epiblast and not as presumptive ectoderm.

A summary of the readily identifiable subpopulations is provided in Fig. 1E, and a direct comparison with the mouse embryo is given in Table S1. Although we do not find exact one-to-one correspondence, and in places our gastruloid classifications are also coarser grained (for example, we do not resolve the three different types of extra-embryonic mesoderm observed in the mouse), we find that there is good overall agreement between the mouse and gastruloid subpopulations.

Cell migration

In addition to the emergence of distinct mesoderm and endoderm subtypes in different anterior-posterior positions along the PS, vertebrate gastrulation is also characterized by highly orchestrated cell migrations. Indeed, fate specification and migration occur concomitantly.

To track populations of cells in our gastruloids we created a clonal cell line that contains the photo-convertible protein KikGR and the far-red histone-localized fluorescent protein RFP657-H2B (Fig. 2A). KikGR protein normally fluoresces green but permanently converts to red upon UV excitation. KikGR also has a long lifetime, enabling the detection of cells in which the protein has been converted to red even after 48 h. This tool allows photo-conversion of cells in specific regions of gastruloids and determination of their location after a window of time. Taking advantage of the radial symmetry of our system, we investigated the movements of cells in three different annular regions: A_1, all cells <50 μm from the colony center; A_2, all cells in a ring >200 μm and <250 μm from the colony center; and A_3, all cells >400 μm from colony center (Fig. 2B,C). To begin each tracking experiment, we first photo-converted and imaged the cells in a region of interest (Fig. 2C, row 1), and then immediately stimulated with either control medium, BMP4, WNT3A, WNT3A+activin or WNT3A+SB. We then imaged the same colonies again at 24 h (Fig. S2A) and at 52 h (Fig. 2C and quantified in D).

We found that, in the unstimulated micropatterns, the photo-converted cells retained their original position (Fig. 2C, rows 1
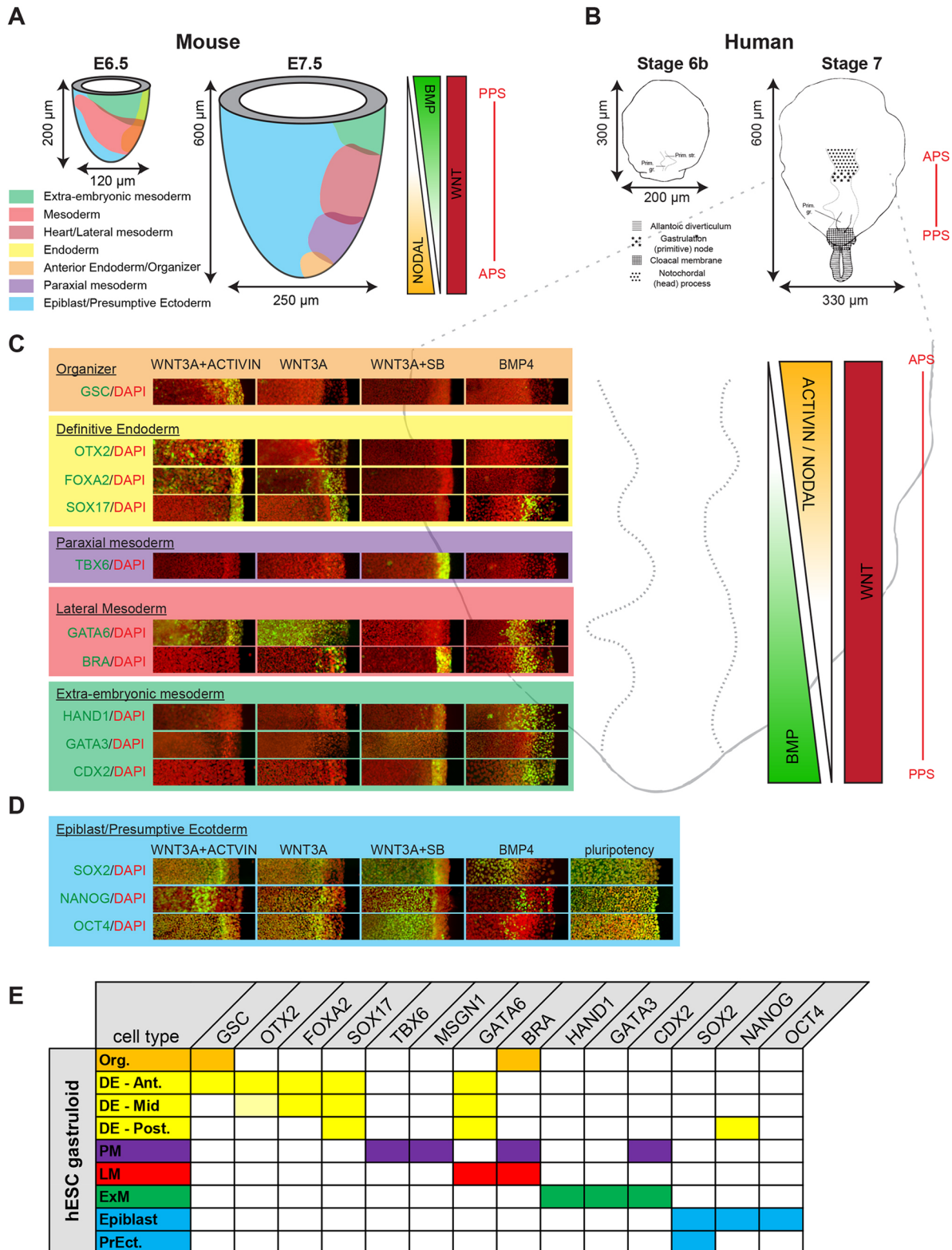
Fig. 1. Mapping gastruloid fates to the human PS. (A) Reproduction of the mouse PS fate map (based on Tam and Behringer, 1997) with inferred signaling gradients of BMP, WNT3A and Nodal (Tam and Loebel, 2007; Arnold and Robertson, 2009). (B) Dorsal representation of the human PS fate map from the Carnegie Collection (O'Rahilly and Müller, 1987). (C) Mapping of gastruloids stimulated with BMP4, WNT3A, WNT3A+SB or WNT3A+activin to the Carnegie Collection stage 7 human PS. Gastruloids were fixed after 48 h and stained for the indicated markers. As each staining is radially symmetric, only a section from r=0 to r=R (500 µm) is shown. (D) Same as C, but comparing the expression profiles of the indicated markers in the differentiation conditions with their expression profiles in pluripotent, undifferentiated micropatterns. (E) Summary of marker expression. The OTX2/DE-Mid box with lighter yellow indicates that expression of OTX2 is less than that observed in other cells in other conditions. APS, anterior PS; DE - Ant., anterior definitive endoderm; DE - Mid, mid-streak definitive endoderm; DE - Post., posterior definitive endoderm; ExM, extra-embryonic mesoderm; LM, lateral mesoderm; Org., organizer; PM, paraxial mesoderm; PPS, posterior PS; PrEct, presumptive ectoderm.
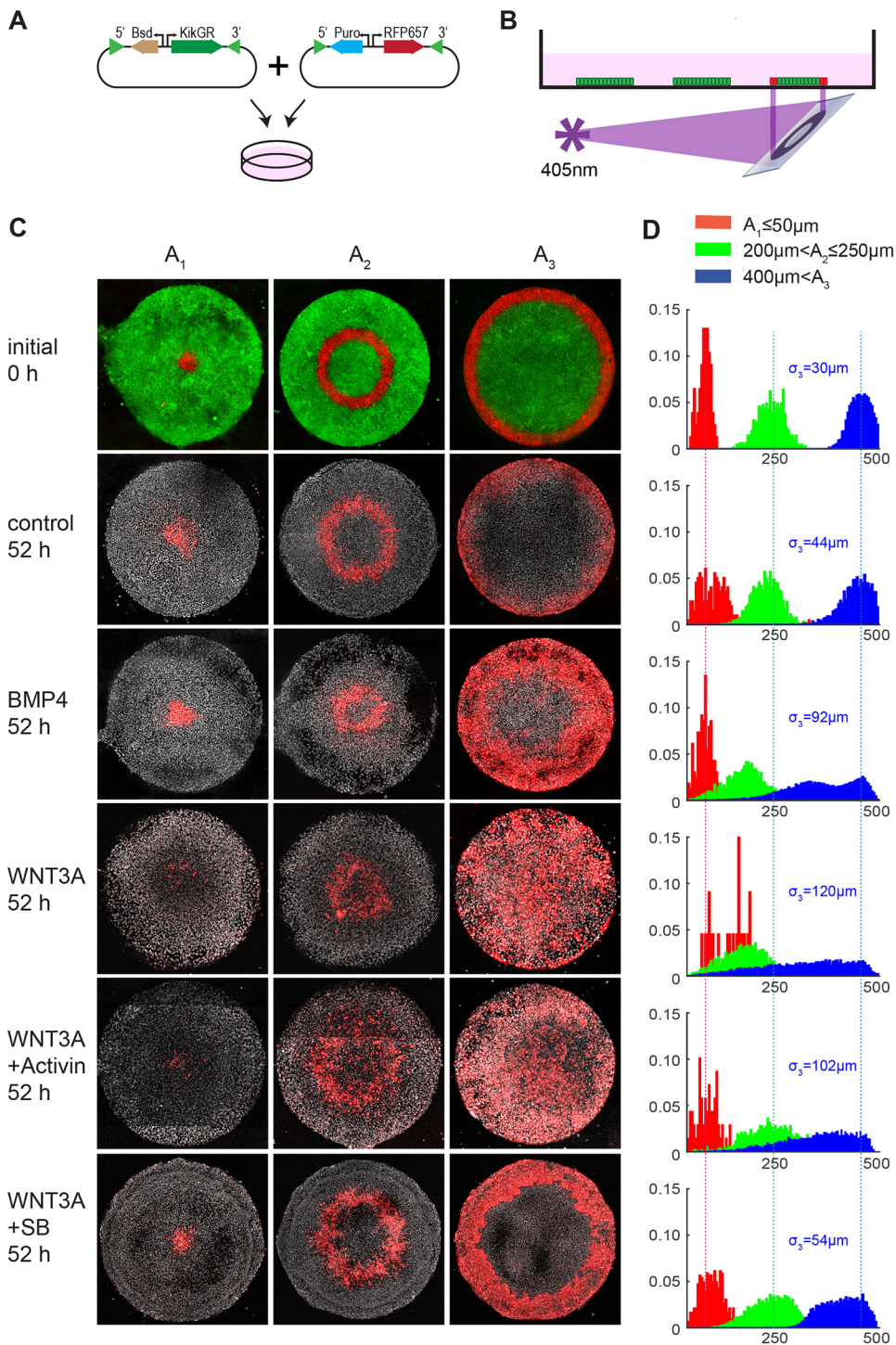
Fig. 2. Directed cell migration in the PS region. (A) Cloning strategy for the RUES2-KiKGR-RFP657-H2B line. (B) Using a digital micromirror, annular regions of 1000 μm diameter micropatterned RUES2-KiKGR-RFP657-H2B colonies were selectively exposed to 405 nm light for 3 s and permanently switched from green to red fluorescence. (C) Row 1 shows unconverted KiKGR fluorescence (green) and converted KiKGR fluorescence (red) at 0 h in each of the three annular regions. All other rows show only converted KiKGR fluorescence (red) and the far-red histone nuclear marker (gray) at 52 h. In all conditions, significant movement of cells in the A_3 region is observed. (D) Quantification of C. To measure the degree of spread of the A_3 region migration in each condition we also computed the root mean square of each A_3 distribution (σ_3, overlaid in blue). Note that this number is not related to the variability or reproducibility of the cell movements, which instead can be inferred from the difference in heights of neighboring bins, as each bin represents an independent sampling of cells. For the A_3 region of each stimulation condition these differences are especially small compared with their respective bin heights, thus showing that the movements are robust. Dotted lines indicate the initial centers of each photoconverted region.

and 2). Stimulation with BMP4, WNT3A, WNT3A+activin or WNT3A+SB, however, led to migration of cells localized at the edge (A_3) towards the center (Fig. 2C, rows 3-6), and the onset of these migrations correlated with the previously reported (Martyn et al., 2018) epithelial-to-mesenchymal transition (EMT) onset observed in each condition (Fig. S3A). Expansion due to differential growth of the outer region compared with the center regions is highly unlikely to be a factor in these movements (Fig. S3B). Under WNT3A and WNT3A+activin stimulation, migration started shortly after 24 h of stimulation and cells migrated in a dispersed, individual manner, travelling long distances from the edge of the colony to the center (Fig. 2C, rows 4 and 5, and Fig. S3). In contrast, a slower, shorter and more compact migration was observed in the BMP4- and WNT3A+SB-induced gastruloids (Fig. S3 and Fig. 2C, D, rows 3 and 6). Quantification of the photo-converted cells in the BMP4 treatment revealed two distinct subpopulations: one that remained on the outer edge, and another that migrated inwards (Fig. 2C,D, row 3). Finally, although no migration was observed in A_1 regardless of the stimulation, cells in the A_2 region shifted slightly inward by 52 h following WNT3A+activin, WNT3A and BMP4 stimulation. However, these cells do not express EMT markers early on (Martyn et al., 2018), and it is hard to differentiate

between active movement and passive movement as the result of being pushed in by the migration of cells from A_3. For example, we speculate that as the A_2 region in BMP4 gastruloids is more compact than in the WNT-treated gastruloids, this is more the result of pushing from the exterior cells rather than autonomous movement.

To better understand how the cells migrate in each condition, we also examined the 3D structure of the gastruloids and what fate markers the migrating cells express (Fig. 3). In the WNT3A and WNT3A+activin gastruloids the migrating cells express SOX17 and so belong to the anterior definitive endoderm subpopulation. In the BMP4 gastruloids the migratory cells express BRA, and so mostly belong to the lateral mesoderm subpopulation. In the WNT3A+SB gastruloids the migratory cells also express BRA and so are the PM-fated cells. In all cases the migrating cells appear to push under the inner epiblast section towards the center of the gastruloid and express the EMT markers SNAIL (SNAI1) and N-cadherin (CDH2). The interaction of these epiblast cells with the migratory cells is also related to the collagen IV layer that we detect separating these layers in the WNT3A, WNT3A+activin and WNT3A+SB gastruloids (Fig. 3C). In the mouse embryo, formation of a collagen IV basement membrane precedes gastrulation, but here it is unclear whether the layer exists before stimulation, or whether it is produced from cells as differentiation proceeds. However, the fact that our layer appears to be patchier than in the embryo and also appears diffusely in the SOX2+ cells suggests that it is produced by the epiblast layer during the course of differentiation (Fig. 3C).

The fact that the observed cell migrations are robust, concurrent with EMT and dependent on the fate the cells adopt, suggests that we are seeing movements indicative of the *in vivo* human gastrulation program. In support of this we note that, in the mouse, the mesoderm cells migrate collectively as a compact tissue (Parameswaran and Tam, 1995; Sutherland, 2016) behind a leading edge of less compact

definitive endoderm progenitors (Viotti et al., 2014; Rivera-Perez and Hadjantonakis, 2014), as this picture is consistent with the rates and behavior of mesoderm and endoderm migrating cells in our gastruloids. In contrast to the in-depth knowledge of cell migration accumulated over the years in the avian PS (Hardy et al., 2008; Yang et al., 2008, 2002; Yue et al., 2008; Sweetman et al., 2008), the mechanisms and chemical cues behind migration in the mammalian PS remain poorly understood (Stankova et al., 2015). We believe that our gastruloid model offers a glimpse of this difficult-to-study *in vivo* process and may present a fruitful alternative approach to dissect the molecular mechanisms underlying cell migration during this pivotal time.

Mapping cell migrations and fates to the human PS

Putting together our gene maps, cell migration patterns and 3D cross-sections, we are able to suggest a detailed graphical representation of what gastrulation may look like in human PS at various anterior-posterior positions (Fig. 4). We propose that the edges of the epiblast/primitive ectoderm (PrEct) region of each gastruloid correspond to the median of the PS, whereas the centers of each gastruloid are positioned laterally relative to this median. In this schema, the direction of migration of differentiating cells is from the medial line of the streak out laterally, underneath the collagen IV and epiblast/PrEct layer. The outermost ring of exposed differentiated cell in the gastruloids would be underneath the epiblast that, in the embryo, persists as a continuous epithelium because of cell proliferation (mouse; Kojima et al., 2014) and flow into the streak (chick; Voiculescu et al., 2014). In the gastruloids, there is nothing anchoring the top inner epiblast layer to the colony boundary, and cellular attachments to the coverslip would inhibit the flows seen in chick. Interestingly, whether the migrating cells go under or over appears to be surface dependent, as in previously published work on poly-dimethyl siloxane (PDMS) micropatterns, the corresponding migratory population appeared on the top of the epiblast
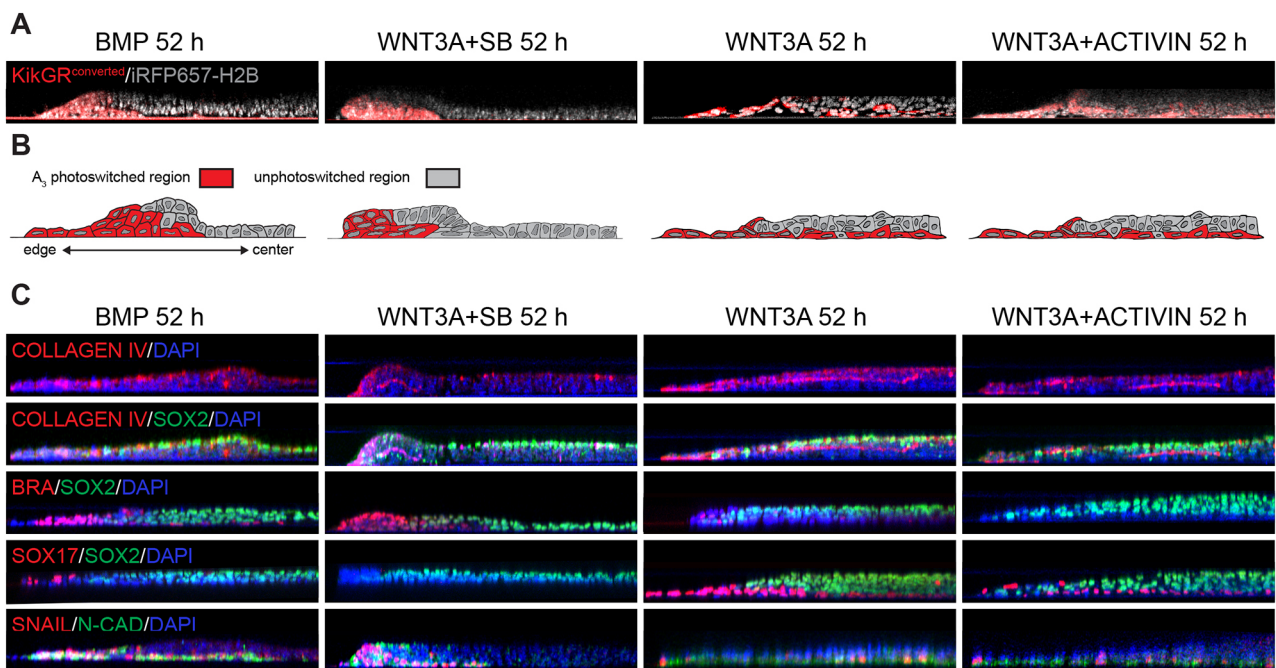

Fig. 3. 3D gastruloid morphology. (A) Radial cross-sections of RUES2-KiKGR-RFP657-H2B micropatterns photo-converted in region A_3 and stimulated with WNT3A, WNT3A+activin, WNT3A+SB or BMP4 for 52 h. In all conditions the photo-converted cells (red) can be seen to be migrating under the inner epiblast or ectoderm-like region (gray). (B) Hand-drawn depiction of 3D structure of gastruloids inferred from A. (C) Radial cross-sections of RUES2 gastruloids stimulated with WNT3A, WNT3A+activin, WNT3A+SB or BMP4, fixed and stained at 52 h for the indicated markers. As can be seen by comparison with A and B, the migratory cells are differentiated to mesoderm or endoderm and express PS markers. One can also see that in all conditions except BMP4 a basement layer of collagen IV separates the bottom migrating cells from the undifferentiated epiblast-like cells on top.
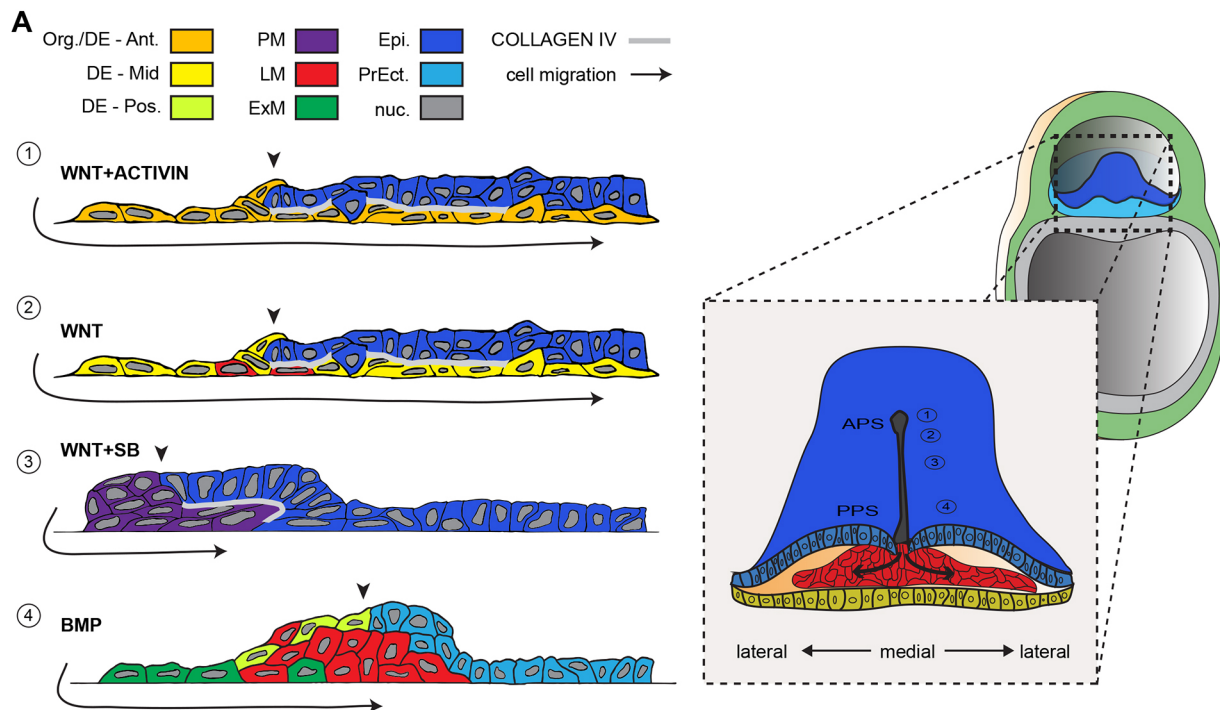
DEVELOPMENT

Fig. 4. Mapping gastruloid cell migrations and fates to the human PS. (A) Diagram summarizing the fates and 3D structure of each type of gastruloid at 52 h and mapping to the human embryo (indicated by positions 1-4). As indicated by the arrowheads, we believe the edge of the epiblast/PrEct region in each gastruloid corresponds to the medial part of the *in vivo* PS, and that our migrations (indicated by arrows) therefore occur medially to laterally. APS, anterior PS; DE - Ant., anterior definitive endoderm; DE - Mid, mid-streak definitive endoderm; DE - Pos., posterior definitive endoderm; Epi., epiblast; ExM, extra-embryonic mesoderm; LM, lateral mesoderm; nuc., nucleus; Org., organizer; PM, paraxial mesoderm; PPS, posterior PS; PrEct, presumptive ectoderm.

(Martyn et al., 2018). We speculate that in both conditions they may be responding to similar cues but taking whichever route is easier depending on attachment of the remaining epiblast/PrEct region to the surface.

There is no doubt that our gastruloid-derived gene/fate map lacks details and features that could be observed in the developing *in vivo* human embryo. We anticipate that missing cell types, such as germ cells or intermediate mesoderm, for example, might be revealed in the future with the use of single cell RNA-seq of gastruloids and sets of markers informed by new efforts to acquire single cell RNA-seq data from gastrulating primate embryos (Nakamura et al., 2017). They might also be revealed by tweaking the ligand concentrations and combinations beyond the simple extremes and combinations explored here. There is also the limitation that, unlike the *in vivo* case, our anterior-posterior streak is a composite of separate differently stimulated gastruloids. That said, given what we have learned about the required stimulation conditions for each fate subpopulation, it may be possible, with advances in micropatterning techniques or localized ligand sources, to recreate the entire anterior-posterior streak in a single micropattern. This would be a superior model and allow much better understanding of the relative timing of EMT, fate specification and migrations. However, regardless of the limitations of our current studies, we believe our results represent a first step towards observing and mapping the origin of fate during our own human development.

MATERIALS AND METHODS
Cell culture
hESCs (RUES2 cell line) were grown and maintained in HUESM medium conditioned by mouse embryonic fibroblasts (MEF-CM) and supplemented with 20 ng/ml bFGF. Testing for mycoplasma was carried out before beginning each set of experiments and again at 2-month intervals. For maintenance conditions, cells were grown on GelTrex-coated (Invitrogen, 1:40 dilution) tissue culture dishes (BD Biosciences). The dishes were coated overnight at 4°C and then incubated at 37°C for at least 10 min before the cells were seeded on the surface. Cells were passaged using Gentle Cell Dissociation Reagent (Stemcell Technologies, 07174).

Micropatterned cell culture
We used micropatterned glass coverslips from CYTOO. The coverslips were first coated with 10 μg/ml laminin 521 (Biolamina) diluted in PBS with calcium and magnesium (PBS++) for 3 h at 37°C. Cells were dissociated with StemPro Accutase (Life Technologies) for 7 min. Cells were then washed once with growth media, washed again with PBS, and then re-suspended in growth media with 10 μM ROCK-inhibitor Y-27632 (Abcam) in 35 mm tissue culture plastic dishes. For each coverslip 1×10^6 cells in 2 ml of media were used. After 1 h, ROCK-inhibitor was removed and was replaced with standard growth media supplemented with Pen-Strep (Life Technologies). Cells were stimulated with the following ligands or small molecules 12 h after seeding: 100 ng/ml WNT3A, 50 ng/ml BMP4, 100 ng/ml activin A or 10 μM SB.

Establishment of stable photo-convertible hESC cell line
pCAG:KikGR was a gift from Anna-Katerina Hadjantonakis (Addgene plasmid #32608). The KikGR protein from this plasmid was amplified with forward primer 5-ATTGGATCCCGGATGGTGAGTGTGATTACATCA-GAA-3 and reverse primer 5-TATGCGGCCGCCGGTTACTTGGCCAG-CCTTG-3 and, using BamHI and NotI cloning sites, was inserted into an ePiggyBac plasmid with a pCAG promoter and puromycin resistance cassette (Lacoste et al., 2009). This plasmid, along with a plasmid carrying the piggybac transposase and another ePiggyBac plasmid carrying a H2B-RFP657 fluorescent protein and blasticidin resistance, were nucleofected into 1×10^6 pluripotent RUES2 cells using the B-016 setting on an Amaxa Nucleofector II (Lonza). Nucleofected cells were then plated as per maintenance conditions, but supplemented with 10uM ROCK-inhibitor. Selection for both puromycin and blasticidin commenced after 2 days, and

ROCK-inhibitor was maintained until colonies reached adequate size (typically 8-16 cells per colony). To derive pure clones, individual colonies were picked in an IVF hood with a 20 µl pipette tip and seeded into separate wells with growth media and ROCK-inhibitor. Once successfully established, each clone was assayed functionally for brightness and homogeneity of the KikGR and H2B-RFP647 fluorescent proteins. Each clone was also assayed functionally for its ability to recapitulate the self-organization in micropatterns when stimulated with BMP4. Three successful clones were selected, and one was used for subsequent studies.

Immunostaining
Cultures were fixed in 4% paraformaldehyde for 20 min, washed twice with PBS, and then blocked and permeabilized with 3% donkey serum and 0.1% Triton X-100 in PBS for 30 min. Cultures were incubated overnight with primary antibodies in this blocking buffer at 4°C (for primary antibodies and dilutions, see Table S2), washed three times with PBS+0.1% Tween-20 for 30 min each, and then incubated with secondary antibodies (Life Technologies: donkey anti-rabbit, donkey anti-mouse or donkey anti-goat antibodies conjugated with Alexa Fluor 488, 555 or 647) and DAPI for 30 min before a final washing with PBS and mounting onto glass slides for imaging.

qPCR data
RNA was collected in Trizol at indicated time points from either micropatterned colonies or from small unpatterned colonies and was purified using the RNeasy mini kit (Qiagen). qPCR was performed as described previously (Etoc et al., 2016) and primer designs are listed in Table S3.

Imaging and image analysis
Images were acquired using a Zeiss Axio Observer and a 20×/0.8 numerical aperture (NA) lens or using a Leica SP8 inverted confocal microscope with a 40×/1.1-NA water-immersion objective. Image analysis and stitching was performed with ImageJ and custom Matlab routines. For tracking cells with the RUES2-KikGR-RFP657-H2B cell line, segmentation was carried out as for fixed cells, except here we used the H2B-RFP647 fluorescence signal instead of a DAPI signal as the nuclear marker. We then trained an Ilastick classifier to binarize cells as photo-converted or unconverted, and binned the converted cells into a radial histogram. The plots in Fig. 2D represent the average of n=5 colonies.

Cell tracking with photo-convertible line
RUES2-KikGR-RFP657-H2B cells were plated onto micropatterned CYTOO chips instead of home-made chips in order to accommodate the 19.5×19.5 mm spaced CYTOO chip holder. Immediately after stimulation with BMP, WNT3A or WNT3A+SB, each chip was sequentially loaded into the CYTOO chip holder, placed on the microscope, photo-converted, washed with PBS and then returned to the culture dish. Photo-conversion was carried out on a custom-built spinning-disk confocal Inverted Zeiss Axiovert 200 microscope with a Photonics Instruments Digital Mosaic system using a 405 nm laser. Regions of interest (ROIs) for photo-conversion were programmed with custom Matlab code and then loaded into the Metamorph software used to operate the microscope. In our case the regions of interest were: A_1, all cells <50 µm from the colony center; A_2, all cells in a ring >200 µm and <250 µm from the colony center; and A_3, all cells >400 µm from colony center. Individual colonies were found, aligned with the ROI and had their stage position stored. Using a custom-written Metamorph script, each colony was sequentially imaged with GFP and RFP filters, exposed to 3162 ms of 405 nm light from the laser, and then imaged again to check for complete photo-conversion. Once photo-converted, each CYTOO chip was returned to its native 35 mm dish and placed in an incubator. For tracking these cells at later times, the micropatterned chips were taken out of the incubator and sequentially re-loaded in the CYTOO holder and imaged with the Leica SP8 confocal microscope (see Imaging and Image Analysis section). They were then washed and returned to the incubator.

References
Alev, C., Wu, Y., Kasukawa, T., Jakt, L. M., Ueda, H. R. and Sheng, G. (2010). Transcriptomic landscape of the primitive streak. *Development* **137**, 2863-2874. doi:10.1242/dev.053462

Arnold, S. J. and Robertson, E. J. (2009). Making a commitment: cell lineage allocation and axis patterning in the early mouse embryo. *Nat. Rev. Mol. Cell Biol.* **10**, 91-103. doi:10.1038/nrm2618

Beck, F., Erler, T., Russell, A. and James, R. (1995). Expression of Cdx-2 in the mouse embryo and placenta: possible role in patterning of the extra-embryonic membranes. *Dev. Dyn.* **204**, 219-227. doi:10.1002/aja.1002040302

Chalamalasetty, R. B., Garriock, R. J., Dunty, W. C., Kennedy, M. W., Jailwala, P., Si, H. and Yamaguchi, T. P. (2014). Mesogenin 1 is a master regulator of paraxial presomitic mesoderm differentiation. *Development* **141**, 4285-4297. doi:10.1242/dev.110908

Chapman, D. L., Agulnik, I., Hancock, S., Silver, L. M. and Papaioannou, V. E. (1996). Tbx6, a mouse T-Box gene implicated in paraxial mesoderm formation at gastrulation. *Dev. Biol.* **180**, 534-542. doi:10.1006/dbio.1996.0326

Conklin, E. G. (1905). The organization and cell lineage of the ascidian egg. *J. Acad. Nat. Sci. Philadelphia* **13**, 1-119. doi:10.5962/bhl.title.4801

Deglincerti, A., Croft, G. F., Pietila, L. N., Zernicka-Goetz, M., Siggia, E. D. and Brivanlou, A. H. (2016). Self-organization of the in vitro attached human embryo. *Nature* **533**, 251-254. doi:10.1038/nature17948

Etoc, F., Metzger, J., Ruzo, A., Kirst, C., Yoney, A., Ozair, M. Z., Brivanlou, A. H. and Siggia, E. D. (2016). A balance between secreted inhibitors and edge sensing controls gastruloid self-organization. *Dev. Cell* **39**, 302-315. doi:10.1016/j.devcel.2016.09.016

Firulli, A. B., Mcfadden, D. G., Lin, Q., Srivastava, D. and Olson, E. N. (1998). Heart and extra-embryonic mesodermal defects in mouse embryos lacking the bHLH transcription factor Hand1. *Nat. Genet.* **18**, 266-270. doi:10.1038/ng0398-266

Hardy, K. M., Garriock, R. J., Yatskievych, T. A., D'agostino, S. L., Antin, P. B. and Krieg, P. A. (2008). Non-canonical Wnt signaling through Wnt5a/b and a novel Wnt11 gene, Wnt11b, regulates cell migration during avian gastrulation. *Dev. Biol.* **320**, 391-401. doi:10.1016/j.ydbio.2008.05.546

Hart, A. H., Hartley, L., Ibrahim, M. and Robb, L. (2004). Identification, cloning and expression analysis of the pluripotency promoting Nanog genes in mouse and human. *Dev. Dyn.* **230**, 187-198. doi:10.1002/dvdy.20034

Hatada, Y. and Stern, C. D. (1994). A fate map of the epiblast of the early chick embryo. *Development* **120**, 2879-2889.

Home, P., Kumar, R. P., Ganguly, A., Saha, B., Milano-Foster, J., Bhattacharya, B., Ray, S., Gunewardena, S., Paul, A., Camper, S. A. et al. (2017). Genetic redundancy of GATA factors in the extraembryonic trophoblast lineage ensures the progression of preimplantation and postimplantation mammalian development. *Development* **144**, 876-888. doi:10.1242/dev.145318

Hyun, I., Wilkerson, A. and Johnston, J. (2016). Embryology policy: revisit the 14-day rule. *Nature* **533**, 169-171. doi:10.1038/533169a

International Society of Stem Cell Research. (2016). *Guidelines for Stem Cell Research and Clinical Translation*. International Society for Stem Cell Research.

Kimmel, C. B., Warga, R. M. and Schilling, T. F. (1990). Origin and organization of the zebrafish fate map. *Development* **108**, 581-594.

Kojima, Y., Tam, O. H. and Tam, P. P. L. (2014). Timing of developmental events in the early mouse embryo. *Semin. Cell Dev. Biol.* **34**, 65-75. doi:10.1016/j.semcdb.2014.06.010

DEVELOPMENT

Koutsourakis, M., Langeveld, A., Patient, R., Beddington, R. and Grosveld, F. (1999). The transcription factor GATA6 is essential for early extraembryonic development. *Development* **126**, 723-732.

Lacoste, A., Berenshteyn, F. and Brivanlou, A. H. (2009). An efficient and reversible transposable system for gene delivery and lineage-specific differentiation in human embryonic stem cells. *Cell Stem Cell* **5**, 332-342. doi:10.1016/j.stem.2009.07.011

Manaia, A., Lemarchandel, V., Klaine, M., Romeo, P. and Godin, I. (2000). Lmo2 and GATA-3 associated expression in intraembryonic hemogenic sites. *Development* **127**, 643-653.

Martyn, I., Kanno, T. Y., Ruzo, A., Siggia, E. D. and Brivanlou, A. H. (2018). Self-organization of a human organizer by combined Wnt and Nodal signalling. *Nature* **558**, 132-135. doi:10.1038/s41586-018-0150-y

Martyn, I., Brivanlou, A. H. and Siggia, E. D. (2019). A wave of WNT signaling balanced by secreted inhibitors controls primitive streak formation in micropattern colonies of human embryonic stem cells. *Development* **146**, dev172791. doi:10.1242/dev.172791

Morgani, S. M., Metzger, J. J., Nichols, J., Siggia, E. D. and Hadjantonakis, A.-K. (2018). Micropattern differentiation of mouse pluripotent stem cells recapitulates embryo regionalized cell fate patterning. *eLife* **7**, e32839. doi:10.7554/eLife.32839

Nakamura, T., Yabuta, Y., Okamoto, I., Sasaki, K., Iwatani, C., Tsuchiya, H. and Saitou, M. (2017). Single-cell transcriptome of early embryos and cultured embryonic stem cells of cynomolgus monkeys. *Sci. Data* **4**, 170067. doi:10.1038/sdata.2017.67

Nowotschin, S., Setty, M., Kuo, Y.-Y., Lui, V., Garg, V., Sharma, R., Simon, C. S., Saiz, N., Gardner, R., Boutet, S. C. et al. (2019). The emergent landscape of the mouse gut endoderm at single-cell resolution. *Nature*, **569** 361-367. doi:10.1038/s41586-019-1127-1

O'Rahilly, R. and Müller, F. (1987). *Developmental Stages in Human Embryos*. Carnegie Institution of Washington.

Parameswaran, M. and Tam, P. P. L. (1995). Regionalisation of cell fate and morphogenetic movement of the mesoderm during mouse gastrulation. *Dev. Genet.* **17**, 16-28. doi:10.1002/dvg.1020170104

Ralston, A., Cox, B. J., Nishioka, N., Sasaki, H., Chea, E., Rugg-Gunn, P., Guo, G., Robson, P., Draper, J. S. and Rossant, J. (2010). Gata3 regulates trophoblast development downstream of Tead4 and in parallel to Cdx2. *Development* **137**, 395-403. doi:10.1242/dev.038828

Rivera-Perez, J. A. and Hadjantonakis, A.-K. (2014). The Dynamics of Morphogenesis in the Early Mouse Embryo. *Cold Spring Harb. Perspect. Biol.* **7**, a015867. doi:10.1101/cshperspect.a015867

Savory, J. G. A., Bouchard, N., Pierre, V., Rijli, F. M., De Repentigny, Y., Kothary, R. and Lohnes, D. (2009). Cdx2 regulation of posterior development through non-Hox targets. *Development* **136**, 4099-4110. doi:10.1242/dev.041582

Sherwood, R. I., Maehr, R., Mazzoni, E. O. and Melton, D. A. (2011). Wnt signaling specifies and patterns intestinal endoderm. *Mech. Dev.* **128**, 387-400. doi:10.1016/j.mod.2011.07.005

Simunovic, M. and Brivanlou, A. H. (2017). Embryoids, organoids and gastruloids: new approaches to understanding embryogenesis. *Development* **144**, 976-985. doi:10.1242/dev.143529

Solnica-Krezel, L. and Sepich, D. S. (2012). Gastrulation: making and shaping germ layers. *Annu. Rev. Cell Dev. Biol.* **28**, 687-717. doi:10.1146/annurev-cellbio-092910-154043

Stankova, V., Tsikolia, N. and Viebahn, C. (2015). Rho kinase activity controls directional cell movements during primitive streak formation in the rabbit embryo. *Development* **142**, 92-98. doi:10.1242/dev.111583

Sutherland, A. E. (2016). Tissue morphodynamics shaping the early mouse embryo. *Semin. Cell Dev. Biol.* **55**, 89-98. doi:10.1016/j.semcdb.2016.01.033

Sweetman, D., Wagstaff, L., Cooper, O., Weijer, C. and Munsterberg, A. (2008). The migration of paraxial and lateral plate mesoderm cells emerging from the late primitive streak is controlled by different Wnt signals. *BMC Dev. Biol.* **8**, 63. doi:10.1186/1471-213X-8-63

Tam, P. P. L. and Behringer, R. R. (1997). Mouse gastrulation: the formation of a mammalian body plan. *Mech. Dev.* **68**, 3-25. doi:10.1016/S0925-4773(97)00123-8

Tam, P. P. L. and Loebel, D. A. F. (2007). Gene function in mouse embryogenesis: get set for gastrulation. *Nat. Rev. Genet.* **8**, 368-381. doi:10.1038/nrg2084

Teo, A. K. K., Arnold, S. J., Trotter, M. W. B., Brown, S., Ang, L. T., Chng, Z., Robertson, E. J., Dunn, N. R. and Vallier, L. (2011). Pluripotency factors regulate definitive endoderm specification through eomesodermin. *Genes Dev.* **25**, 238-250. doi:10.1101/gad.607311

Van Den Brink, S. C., Baillie-Johnson, P., Balayo, T., Hadjantonakis, A.-K., Nowotschin, S., Turner, D. A. and Martinez Arias, A. (2014). Symmetry breaking, germ layer specification and axial organisation in aggregates of mouse embryonic stem cells. *Development* **141**, 4231-4242. doi:10.1242/dev.113001

Viotti, M., Nowotschin, S. and Hadjantonakis, A.-K. (2014). SOX17 links gut endoderm morphogenesis and germ layer segregation. *Nat. Cell Biol.* **16**, 1146-1156. doi:10.1038/ncb3070

Vogt, W. (1929). Gestaltungsanalyse am Amphibienkeim mit Örtlicher Vitalfärbung. *Wilhelm Roux. Arch. Entwickl. Mech. Org.* **120**, 384-706. doi:10.1007/BF02109667

Voiculescu, O., Bodenstein, L., Lau, I.-J. and Stern, C. D. (2014). Local cell interactions and self-amplifying individual cell ingression drive amniote gastrulation. *eLife* **3**, e01817. doi:10.7554/eLife.01817

Warmflash, A., Sorre, B., Etoc, F., Siggia, E. D. and Brivanlou, A. H. (2014). A method to recapitulate early embryonic spatial patterning in human embryonic stem cells. *Nat. Methods* **11**, 847-854. doi:10.1038/nmeth.3016

Yang, X., Dormann, D., Münsterberg, A. E. and Weijer, C. J. (2002). Cell movement patterns during gastrulation in the chick are controlled by positive and negative chemotaxis mediated by FGF4 and FGF8. *Dev. Cell* **3**, 425-437. doi:10.1016/S1534-5807(02)00256-3

Yang, X., Chrisman, H. and Weijer, C. J. (2008). PDGF signalling controls the migration of mesoderm cells during chick gastrulation by regulating N-cadherin expression. *Development* **135**, 3521-3530. doi:10.1242/dev.023416

Yoon, J. K., Moon, R. T. and Wold, B. (2000). The bHLH class protein pMesogenin1 can specify paraxial mesoderm phenotypes. *Dev. Biol.* **222**, 376-391. doi:10.1006/dbio.2000.9717

Yue, Q., Wagstaff, L., Yang, X., Weijer, C. and Munsterberg, A. (2008). Wnt3a-mediated chemorepulsion controls movement patterns of cardiac progenitors and requires RhoA function. *Development* **135**, 1029-1037. doi:10.1242/dev.015321

DEVELOPMENT